Experimental and theoretical investigation on interactions between xylose-containing hemicelluloses and procyanidins

Xuwei Liu, Jiayi Li, Agnès Rolland-Sabaté, Serge Perez, Carine Le Bourvellec, Catherine M.G.C. Renard

HAL Id: hal-03532362
https://hal.inrae.fr/hal-03532362

Submitted on 22 Jul 2024

Experimental and theoretical investigation on interactions between xylose-containing hemicelluloses and procyanidins

Xuwei Liu[a,b], Jiayi Li[c], Agnès Rolland-Sabaté[b], Serge Perez[d], Carine Le Bourvellec[b]*, Catherine M.G.C. Renard[b,e]

[a]College of Food Science, South China Agricultural University, 483 Wushan Road, Guangzhou 510642, China

[b]INRAE, Avignon University, UMR408 SQPOV, F-84000 Avignon, France

[c]State Key Laboratory of Microbial Metabolism, Joint International Research Laboratory of Metabolic & Developmental Sciences, School of Life Sciences & Biotechnology, Shanghai Jiao Tong University, 200240 Shanghai, China

[d]CNRS, CERMAV, University Grenoble Alpes, 38000 Grenoble, France

[e]INRAE, TRANSFORM, F-44000 Nantes, France

Corresponding authors*

Carine Le Bourvellec (carine.le-bourvellec@inrae.fr)

INRAE, UMR408 SQPOV « Sécurité et Qualité des Produits d'Origine Végétale » 228 route de l'Aérodrome

CS 40509

F-84914 Avignon cedex 9

Tél: +33 (0)4 32 72 25 35

Fax: +33 (0)4 32 72 24 92

Others authors

Xuwei Liu: liuxwell@126.com; xuwei.liu@scau.edu.cn

Jiayi Li: jemmylee@sjtu.edu.cn

Agnès Rolland-Sabaté: agnes.rolland-sabate@inrae.fr

Serge Perez: spsergeperez@gmail.com

Catherine M.G.C Renard: catherine.renard@inrae.fr

Graphical Abstract
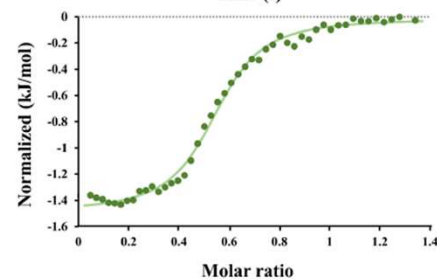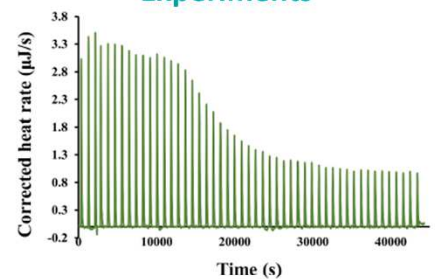
Experiments
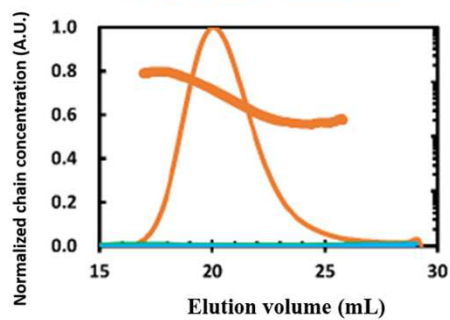
Computational simulations

Hemicellulose

Structural optimizations

Molecular electrostatic potential

ESP/a.u.
0.04
-0.04

Hemicellulose

Procyanidin

HPSEC-MALLS chromatograms

Interaction region

δg index /a.u.
3.0
0.0

Complexes

Mutually exclusive forces

Van del Waals interaction

Hydrogen bonding

Sign(λ₂)ρ/ a.u.
0.05
-0.05

2
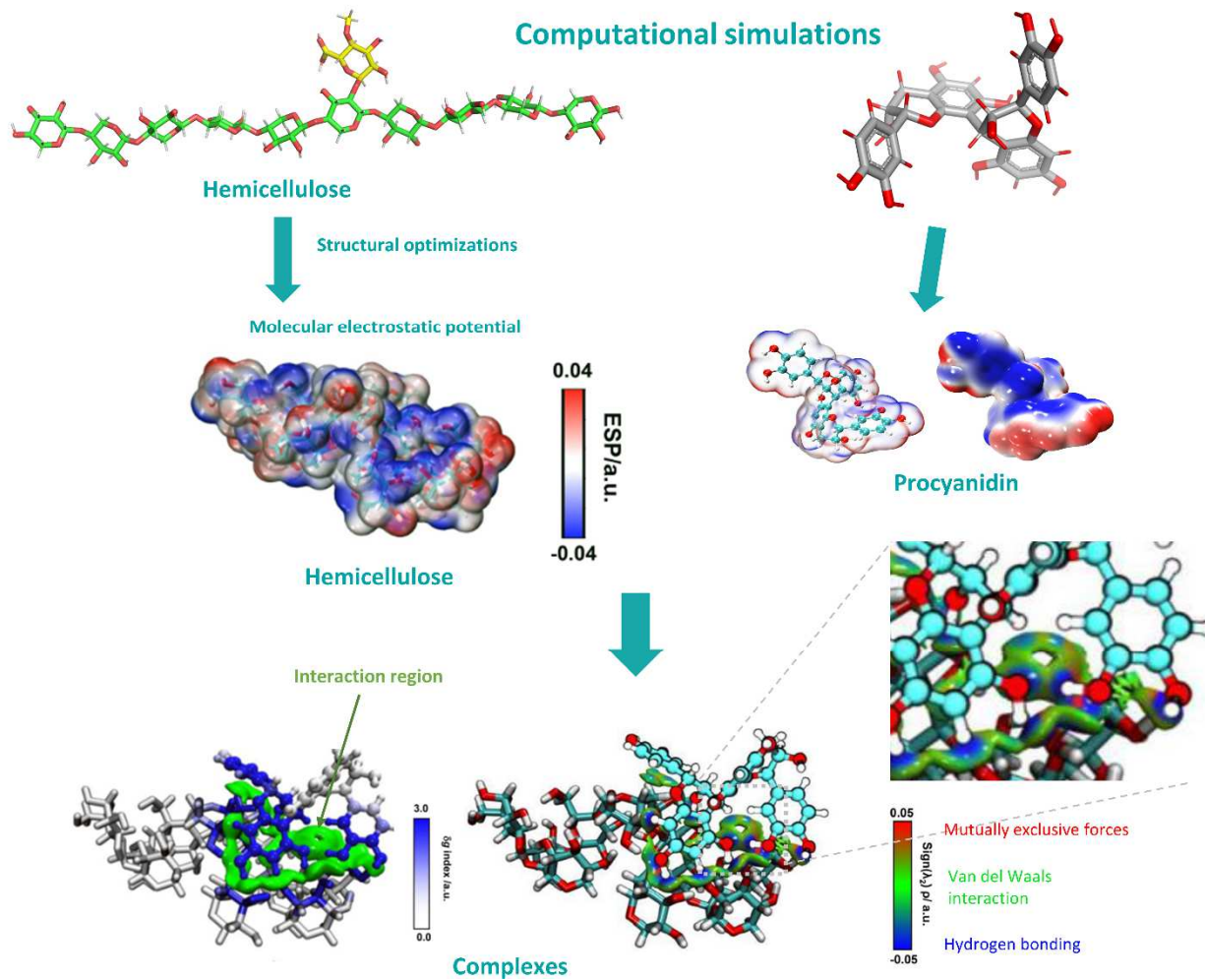
1   **Abstract**

2   During processing of plant-based foods, cell wall polysaccharides and polyphenols,

3   such as procyanidins, interact extensively, thereby affecting their physicochemical

4   properties along with their potential health effects. Although hemicelluloses are

5   second only to pectins in affinity for procyanidins in cell walls, a detailed study of

6   their interactions lacks. We investigated the interactions between representative

7   xylose-containing water-soluble hemicelluloses and procyanidins. Turbidity, ITC and

8   DLS were used to determine the relative affinities, and theoretical calculations further

9   ascertained the interactions mechanisms. Xyloglucan and xylan exhibited respectively

10   the strongest and weakest interactions with procyanidins. The different arabinoxylans

11   interacted with procyanidins in a similar strength, intermediate between xyloglucans

12   and xylans. Therefore, the strength of the interaction depended on the structure itself

13   rather than on some incidental properties, e.g., viscosity and molar mass. The

14   arabinose side-chain of arabinoxylan did not inhibit interactions. The computational

15   investigation corroborated the experimental results in that the region of interaction

16   between xyloglucan and procyanidins was significantly wider than that of other

17   hemicelluloses.

18   **Keywords:** Condensed tannin; Polysaccharide; Xyloglucan; Noncovalent binding;

19   ITC; Molecular simulation

20   **Abbreviations:**

21   HPSEC-MALLS, High Performance Size-Exclusion Chromatography coupled with

22   Multi-Angle Laser Light Scattering; ITC, Isothermal Titration Calorimetry; DLS,

23   Dynamic Light Scattering; $\overline{DP_n}$, number average Degree of Polymerization; $\overline{M}_w$,

24   weight-average molar mass; IGM, Independent Gradient Model; VMD, Visual

25   Molecular Dynamics.

1. Introduction

The polyphenols in fruits and vegetables display many potential biological activities, and their dietary intake is related to a reduced risk of suffering from a variety of chronic diseases (Koch, 2019). In addition to some endogenous factors, such as microbiota and related digestive enzymes, food substrates (e.g., dietary fiber) can also significantly regulate their bioavailability and further metabolism (Seal, Courtin, Venema, & de Vries, 2021). In general, most of the ingested polyphenols, especially the macromolecular polyphenols (e.g., procyanidins) are non-bioavailable in the stomach and small intestine. These unabsorbed polyphenols can be transported to the colon by dietary fiber, where bacteria may metabolize them as bioavailable simple phenolic acids (Cui et al., 2019). This process may mediate the potential beneficial effects of dietary fiber-polyphenol complexes, as they or their catabolites may be absorbed and utilized by the human body (Jakobek & Matić, 2019; Le Bourvellec et al., 2019). Therefore, the interactions between dietary fibers and polyphenols may affect the bioavailability of polyphenols.

Among the dietary fibers, hemicelluloses have not benefited from significant attention. They are heteropolysaccharides, such as xylan, arabinoxylan and xyloglucan, including various sugar monomers. They have a moderate affinity with polyphenols in cell walls. Hence, the affinity of procyanidins is greatest for pectins followed by xyloglucan, and lowest for cellulose (Le Bourvellec, Bouchet, & Renard, 2005). In addition, by a step-wise removal of pectins and hemicelluloses in the grape cell wall or apple cell wall, the binding capacity of proanthocyanidins to the

48 remaining cell walls is significantly reduced (Le Bourvellec, Watrelot, Ginies, Imberty,

49 & Renard, 2012; Ruiz-Garcia, Smith, & Bindon, 2014), but cell walls still have an

50 affinity for proanthocyanidins. However, Phan, Flanagan, D'Arcy, & Gidley (2017)

51 compared the selection of different cellulose-based composite materials (cellulose,

52 cellulose-xyloglucan, cellulose-arabinoxylan, cellulose-pectin) for the adsorption

53 capacity of polyphenols. They found that cellulose is the main binder, whereas

54 hemicelluloses (e.g., xyloglucan and arabinoxylan) do not contribute to the adsorption

55 of catechins (Phan et al., 2017). Therefore, the adsorption capacity of specific

56 polysaccharides to specific polyphenols differs. The knowledge of the nature of the

57 interaction occurring between different hemicelluloses and polyphenols still needs

58 clarification.

59 Polyphenols constitute a large group of plant compounds, mainly divided into

60 phenolic acids, flavonoids, stilbenes, and lignans. Procyanidins are the most abundant

61 macromolecular antioxidants in food and diet (Liu, Le Bourvellec, Guyot, & Renard,

62 2021; Saura-Calixto & Pérez-Jiménez, 2018). They are primarily composed of

63 (-)-epicatechin units. Their number average degree of polymerization ($\overline{DP_n}$) varies

64 significantly between species and cultivars. Generally, the ability of polysaccharides

65 to interact with procyanidins is directly proportional to their molecular weight, that is,

66 $\overline{DP_n}$ (Liu, Le Bourvellec, & Renard, 2020; Renard, Watrelot, & Le Bourvellec, 2017).

67 While the interactions between pectins and procyanidins have been thoroughly

68 studied (Liu et al., 2020; Liu, Renard, Bureau, & Le Bourvellec, 2021; Liu, Renard,

69 Rolland-Sabaté, & Le Bourvellec, 2021; Watrelot, Le Bourvellec, Imberty, & Renard,

70 2014), the corresponding knowledge for hemicelluloses, which are the other main

71 non-cellulosic component in the cell walls, is limited. Notably, the relative binding

72 capacity of various hemicellulose components, along with affinity and binding

73 mechanism, remains to be resolved. Therefore, the present study aims to explore the

74 interaction mechanism occurring between hemicelluloses and procyanidins using a

75 combination of techniques including isothermal titration calorimetry (ITC), UV-Vis

76 spectroscopy, high performance size-exclusion chromatography coupled with

77 multi-angle laser light scattering (HPSEC-MALLS) and dynamic light scattering

78 (DLS). In complement, the reactive sites of procyanidins and different hemicelluloses,

79 where explored using the density functional theory (DFT) level, through electrostatic

80 potential (ESP) and frontier molecular orbital (FMO) analysis. Further conformational

81 analysis of intra and intermolecular interactions provided detailed insights about the

82 nature and the strength of the mechanism underlying the interactions between

83 procyanidins and hemicelluloses. The present study contributes to the understanding

84 of the effects of structure, molar mass, viscosity and side chains on interactions

85 through probing the binding of selected procyanidins to different types of

86 hemicellulose components: xylan, xyloglucan and five arabinoxylans. This set of

87 results provides a reference for further study on the effect of the whole plant cell wall

88 system on the bioavailability of procyanidins to better understand the underlying

89 implications of both human nutrition and health interactions.

90 **2. Materials and methods**

91 **2.1. Standards and Chemicals**

6

92   The standards of arabinose, mannose, glucose, fucose, xylose, rhamnose, and

93   galactose were obtained from Fluka (Buchs, Switzerland). Arabinoxylan (Wheat flour)

94   with low /medium/high viscosity, arabinoxylan with 30% and 22% arabinose content,

95   xyloglucan (Tamarind), and xylan (Beechwood) were purchased from Megazyme

96   (Bray, Ireland).

97   **2.2. Procyanidins preparation**

98   Procyanidins (DP9 and DP39) were prepared from two apple varieties ('Marie

99   Menard' and 'Avrolles'), respectively, as described in Liu, Renard, Rolland-Sabaté, &

100   Le Bourvellec (2021). Briefly, aqueous acetone fractions were collected after washing

101   by hexane and methanol, and then purified using a LiChrospher 100 RP-18 (12 μm,

102   Merck, Darmstadt, Germany) column and further characterized following the

103   principles described by Guyot, Marnet, Sanoner, & Drilleau, (2001). The procyanidins

104   contained about 800 mg/g of phenolic compounds, primarily procyanidins plus traces

105   of (−)-epicatechin, 5′ -caffeoylquinic acid, p-coumaroylquinic acid, phloridzine, and

106   flavonols (Supplementary Table 1).

107   **2.3. Macromolecular characteristics of hemicelluloses**

108   Macromolecular features of initial (2.5 g/L) and free hemicelluloses were

109   detected by HPSEC-MALLS as described by Liu, Renard, Rolland-Sabaté, Bureau, &

110   Le Bourvellec (2021). Briefly, samples (100 μL) after being filtered were injected in a

111   Shimadzu series LC system including a diode array detector (DAD), a refractive

112   index detector (RID) (Shimadzu, Kyoto, Japan), and a MALLS (DAWN HELEOS 8+,

113   equipped with a K5 flow cell and a GaAs laser at λ = 660 nm) from Wyatt Technology

Co. (Santa Barbara, CA, USA). Hemicelluloses were separated on PolySep-GFC-P3000, P5000 and P6000 300 × 7.8 mm columns (40 ° C) equipped with a guard column from Phenomenex (Le Pecq, France) eluted by citrate/phosphate buffer (0.1 M, pH 3.8) at 0.6 mL/min. Zimm fitting method with a one order polynomial fit was used to calculate the weight-average molar mass ($\bar{M}_w$) (Rolland-Sabaté, Colonna, Potocki-Véronèse, Monsan, & Planchot, 2004). A refractive index increment (dn/dc) value of 0.146 mL/g was used to calculate the concentration of hemicelluloses. Astra software® (version 7.1.4, Wyatt Technology Co.) was used to calculate and analyze the results. Injections were carried out in duplicates.

2.4. Isothermal titration calorimetry

The entropy and enthalpy changes of procyanidins binding to hemicelluloses were measured in a citrate/phosphate buffer (0.1 M, pH 3.8) at 25 °C with stirring at 90 rev/min, using a TAM III isothermal microcalorimeter (TA instruments, New Castle, USA) as described by Liu, Renard, Rolland-Sabaté, & Le Bourvellec (2021). The hemicellulose samples (15 mM xylose equivalent, a similar concentration for xyloglucan, ca. 3.75 g/L) were injected into an 850 μL sample cell of stainless steel and equilibrated until the baseline was stable. Over 20 min time intervals, 50 injections of 5 μL procyanidins (30 mmol/L in (-)-epicatechin equivalent) were titrated into the sample cell. The raw ITC data, measured as the heating power input against time, were collected continuously and peak integration was fitted by TAM assistant software (NanoAnalyze 3.10.0). The experiments were carried out in

136   duplicates.

2.5. Phase diagram

138   A spectrophotometric method was used to study hemicellulose-procyanidin

139   interactions as described by Liu, Renard, Rolland-Sabaté, & Le Bourvellec (2021).

140   The absorbance values were collected using a SAFAS flx-Xenius XM

141   spectrofluorimeter (SAFAS, Monaco) at 650 nm on a 96-well microplate. Each

142   experiment was performed in triplicate, and the data were recorded at 25 ºC, in a

143   citrate/phosphate buffer (0.1 M, pH 3.8). A serial procyanidin solutions (0, 0.06, 0.12,

144   0.24, 0.46, 0.94, 1.875, 3.75, 7.5, 15, 30 and 60 mmol/L (-)-epicatechin equivalent)

145   and hemicellulose solutions (0, 0.03, 0.06, 0.117, 0.47, 1.875, 7.5 and 30 mmol/L

146   xylose equivalent, a similar concentration for xyloglucan) were prepared along the

147   lines and columns, respectively. Each procyanidin/hemicellulose mixture was

148   prepared by mixing a constant volume of procyanidin and hemicellulose solutions (50

149   µL). The mixture was stirred for 20 s before each measurement. After the test,

150   microplates were centrifuged 10 min at 2100×g. Free procyanidins and hemicelluloses

151   were collected in the supernatant and then analyzed by HPLC-DAD with

152   thioacidolysis and HPSEC-MALLS, respectively.

2.6. Theoretical calculation method

154   The initial structures of monosaccharides (rhamnose, arabinose, xylose, mannose,

155   glucose) and procyanidin B2 were download from PubChem Compound database

156   (https://pubchem.ncbi.nlm.nih.gov/). Five structure of hemicelluloses (AXHB:

157   arabinoxylan (38% Ara), AXMB: arabinoxylan (30% Ara), AXLB: Arabinoxylan (22%

158 Ara), Xyloglucan, Xylan were built using Polys-Glycan Builder (Pérez & Rivet, 2021)

159 and displayed using SweetUnitMol software (Pérez, Tubiana, Imberty, & Baaden,

160 2015). Structural optimizations were obtained at the B3LYP-D3/6-31+G** level.

161 Single-point energy calculations were performed on the optimized structures using a

162 larger basis set standard Pople style, 6-311+G(d,p) basis sets and SMD solvation

163 model correction. As for the five different hemicelluloses, PM7 method was applied

164 to optimize these initial geometries in a rough level, and Gaussian 16 (Frisch et al.,

165 2016) software was adopted to obtain the precise geometries at a level of B3LYP-D3

166 /6-31+G**.

167   Since conformational space increases rapidly with degrees of freedom in small

168 molecules, we conducted modeling studies of samples based on an efficient

169 conformer search algorithm developed by the Grimme group, which can provide

170 adequate sampling of the conformational space. Possible initial geometries were

171 generated using xtb software (Grimme, Bannwarth, & Shushkov, 2017). All the

172 lowest-energy conformations were obtained with the conformer rotamer ensemble

173 sampling tool (CREST) (Pracht, Bohle, & Grimme, 2020) and Molclus program (Lu

174 et al., 2020), respectively (See details in the Supporting Information). Then,

175 non-covalent interaction (NCI) analysis was carried out (additional notes in the

176 Supporting Information). Frontier Molecular Orbital (FMO) analysis (Huang et al.,

177 2020) and Electrostatic potential (ESP) analysis were finally performed by Multiwfn

178 3.7 software package (Lu & Chen, 2012).

179 **2.7. Statistical analysis**

180   All chemical analyses are expressed as mean values of analytical duplicates and

181 triplicates, and the reproducibility of the results is presented as pooled standard

182 deviations (Pooled SD) (Box, Hunter, & Hunter, 1978). Heatmap analyses were

183 performed using Python software (version 3.6) with Seaborn package (Waskom,

184 2014).

185 **3. Results and discussion**

186 **3.1. Characterization of hemicelluloses**

187   Table 1 lists the compositions and structures of the hemicelluloses, whereas

188 Figure 1 displays their molar mass and size distributions. Arabinoxylan (low viscosity)

189 (AXLV), arabinoxylan (medium viscosity) (AXMV) and arabinoxylan (high viscosity)

190 (AXHV) have similar sugar compositions, e.g., arabinose content (35 %), and their

191 molar mass increase with their viscosity (from 2.2 to 3.9 x 10^5 g/mol). Moreover, to

192 compare the influence of the arabinose substitution on their interaction with

193 procyanidins, arabinoxylans with different arabinose contents were introduced, i.e.,

194 with 30% arabinose substituents (AXMB) and with 22% (AXLB): AXMB exhibited a

195 molar mass similar to AXMV whereas AXLV showed a ten times lower molar mass.

196 The addition of xyloglucan (XYLO) and xylan (XYLA) allowed the comparison of

197 the effect of xylose-containing hemicelluloses on procyanidin interactions. XYLO

198 exhibited the highest molar mass, while AXLB showed the lowest (Table 1). The

199 molar mass of xylan was not applicable due to possible interaction with the column.

200 **Table 1.** Neutral sugar compositions (mg/g dry weight) and weight-average molar mass ($\times 10^3$ g/mol) of hemicelluloses.

Samples	Rha	Fuc	Ara	Xyl	Man	Gal	Glc	Total	$\overline{M}_w$
AXLV	1	0	331	608	3	8	5	955	222
AXMV	1	0	335	636	2	6	3	984	261
AXHV	1	0	343	641	0	2	3	990	391
AXMB	1	0	288	693	0	7	5	995	257
AXLB	1	0	209	733	0	6	5	954	24
XYLO	1	0	12	282	140	0	399	834	774
XYLA	12	0	6	716	10	0	8	753	NA
Pooled SD	*0.7*	*0*	*3.3*	*17.2*	*1.1*	*0.4*	*5.3*	*23.1*	*19.6*

201 Rha: rhamnose, Fuc: fucose, Ara: arabinose, Xyl: xylose, Man: mannose, Gal: galactose, Glc: glucose. $\overline{M}_w$, weight-average molar mass. AXLV: Arabinoxylan (low
202 viscosity); AXMV: Arabinoxylan (medium viscosity); AXHV: Arabinoxylan (high viscosity); AXMB: Arabinoxylan (30% Ara); AXLB: Arabinoxylan (22% Ara);
203 XYLO: Xyloglucan; XYLA: Xylan. Pooled SD: pooled standard deviation. NA: Not applicable.
204
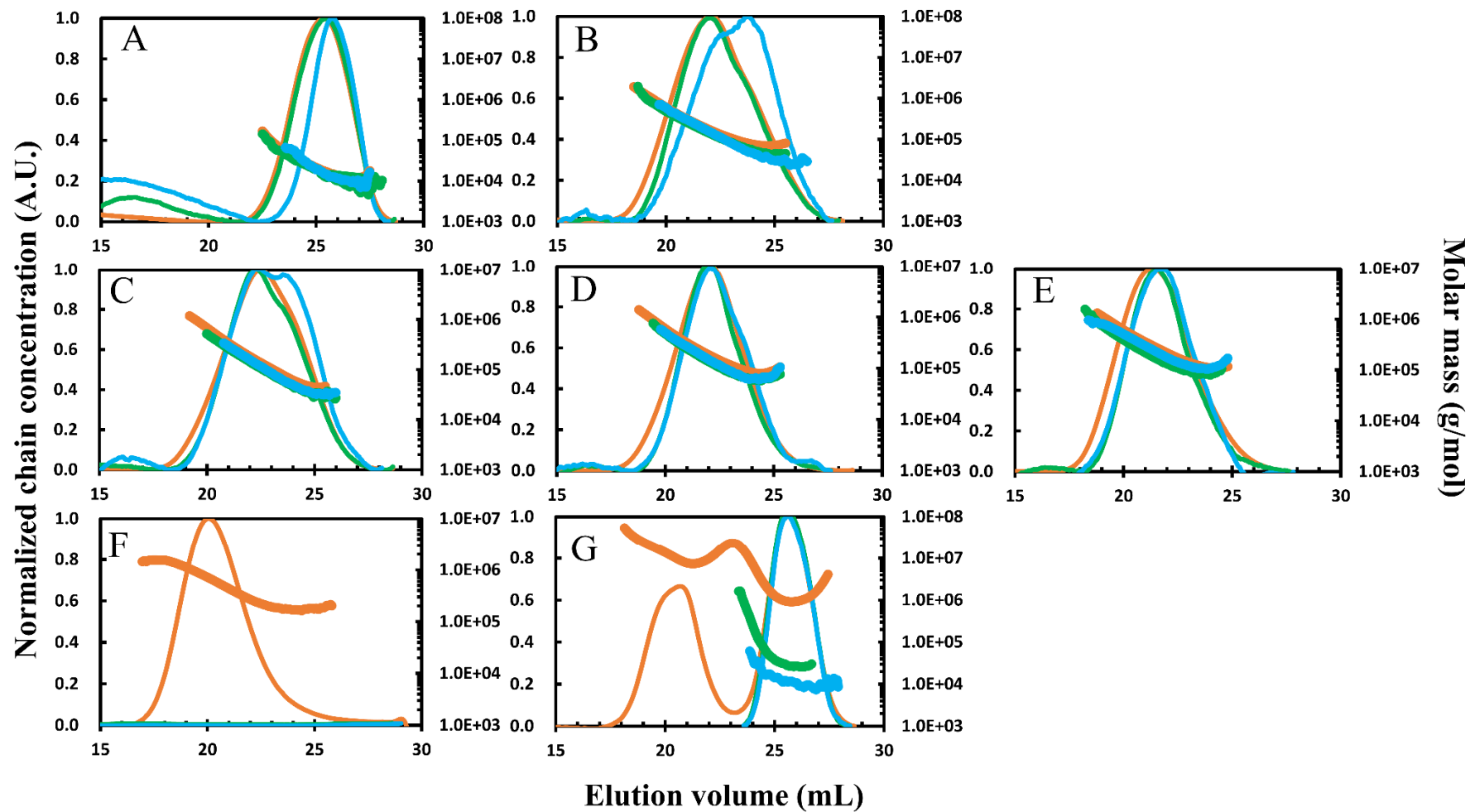
Fig. 1. HPSEC-MALLS chromatograms and molar mass *vs* elution volume for the hemicellulose samples. A, B, C, D, E, F and G: AXLB, AXMB, AXLV, AXMV, AXHV, XYLO and XYLA, respectively. ⎯⎯, ⎯⎯ and ⎯⎯: normalized chain concentration of hemicelluloses before interaction, after interaction with DP9 and DP 39,

208 respectively; ▬, ▬ and ▬ : molar mass of hemicelluloses before interaction, after interaction with DP9 and DP 39. AXLB: Arabinoxylan (22% Ara); AXMB:

209 Arabinoxylan (30% Ara); AXLV: Arabinoxylan (low viscosity); AXMV: Arabinoxylan (medium viscosity); AXHV: Arabinoxylan (high viscosity); XYLO: Xyloglucan;

210 XYLA: Xylan.

3.2. Phase diagram

Turbidity analysis is an effective method for the direct detection of interactions; the increase in turbidity is proportional to the number and size of the complexes (Watrelot, Le Bourvellec, Imberty, & Renard, 2013; Watrelot et al., 2014). The turbidity of the xyloglucan mixture containing procyanidin DP9 increased significantly with increasing xyloglucan concentration (Fig. 2A). However, there was minimal change for the hemicelluloses with a xylan backbone, with an increase only at 30 mM xylose equivalents. Similarly, the absorbance of xyloglucan at the highest concentration increased with increasing procyanidin DP9 concentration (Figure 2B), while the hemicelluloses with a xylan backbone remained constant, which was consistent with the trend in Fig. 2A. The overall aggregation capacity of hemicelluloses (AXHV, AXMV, AXLV, AXMB, AXLB and xylan) with procyanidin DP9 was lower than that of pectins, but the aggregation capacity of xyloglucan with procyanidin DP9 was the same as that of kiwifruit pectins (Liu, Renard, Rolland-Sabaté, & Le Bourvellec, 2021).

Interaction between hemicelluloses and procyanidin DP39 produced significantly more aggregates than with DP9 (Fig. 2 C and D), the turbidity increased significantly with increasing concentrations of either hemicellulose or procyanidin for all the hemicelluloses tested, indicating a strong interaction with procyanidin DP39. The addition of procyanidin DP39 also resulted in a significant increase in the particle diameter of complexes determined by DLS (Supplementary Table 2). Procyanidin DP39, rich in ortho phenolic groups and aryl rings, leads to a more extensive

15

233   aggregation of colloidal particles. The turbidity for hemicelluloses with procyanidins
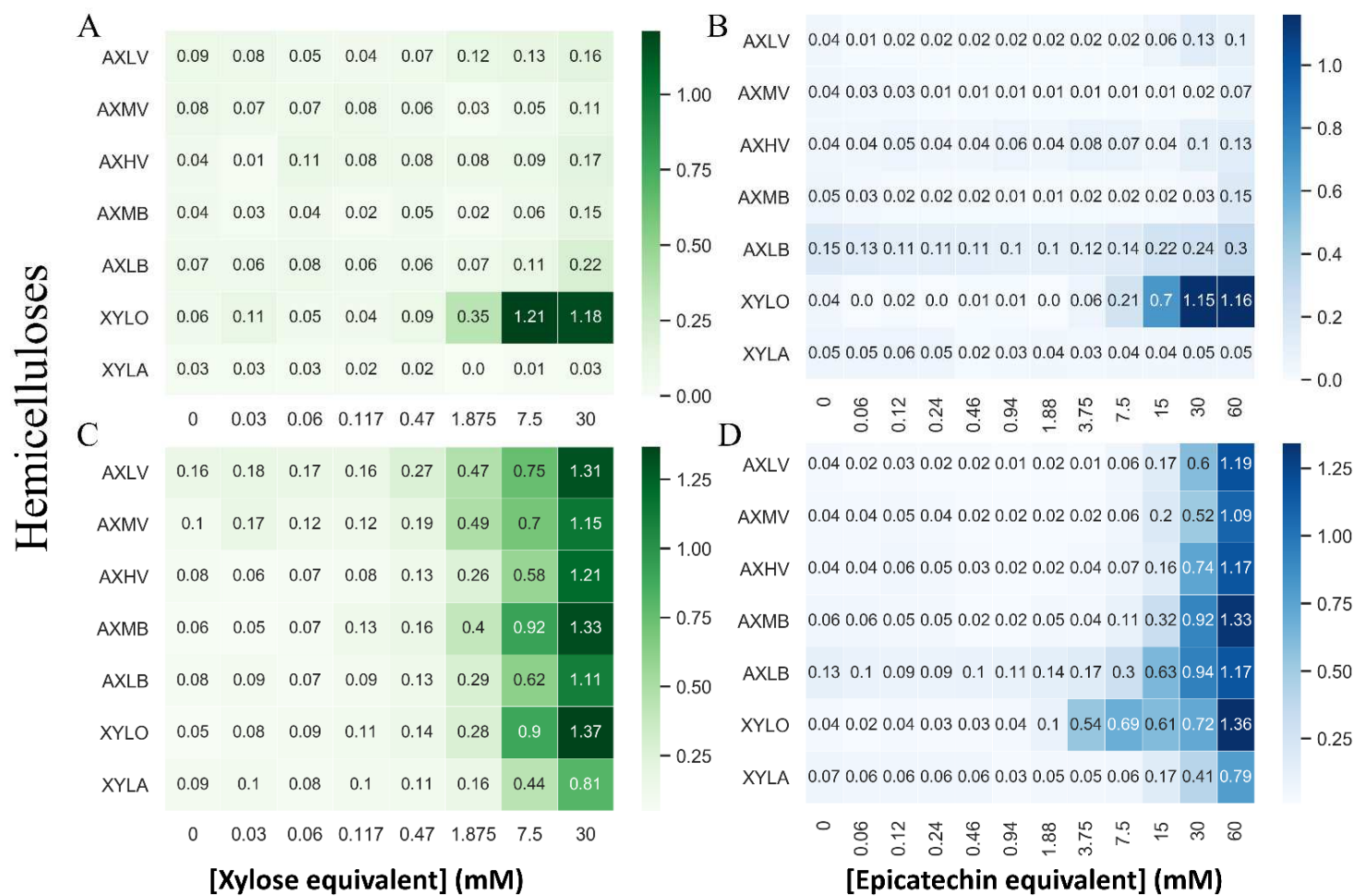
Fig. 2. Heat map of the turbidity characteristics of interactions between hemicelluloses and procyanidins DP9/39. Absorbance at 650 nm, 25 °C, pH 3.8, 0.1 M, citrate/phosphate buffer. (A) and (C): Variation of absorbance of hemicelluloses at different concentrations (xylose equivalent, a similar concentration for xyloglucan) with

237 procyanidins DP9/39 (60 mM epicatechin equivalent). (B) and (D)Variation of absorbance of procyanidins DP9/39 (epicatechin equivalent) at different concentrations with

238 hemicelluloses (30 mM xylose equivalent, a similar concentration for xyloglucan: 7.5 g/L). AXLB: Arabinoxylan (22% Ara); AXMB: Arabinoxylan (30% Ara); AXLV:

239 Arabinoxylan (low viscosity); AXMV: Arabinoxylan (medium viscosity); AXHV: Arabinoxylan (high viscosity); XYLO: Xyloglucan; XYLA: Xylan. The experiments were

240 done in triplicates.

241

242 DP39 at 30 mM xylose equivalent (a similar concentration for xyloglucan: 7.5 g/L) or

243 60 mM (-)-epicatechin equivalent increased in the following order: Xylan < AXLB

244 $\approx$ AXMV $\approx$ AXHV $\approx$ AXLV < AXMB < Xyloglucan. Therefore, xyloglucan

245 had the strongest aggregation capacity with procyanidins, followed by arabinoxylan

246 and xylan had the weakest aggregation capacity. The different types of arabinoxylans

247 had similar capacities. This result was consistent with the results of DLS

248 (Supplementary Table 2): the size of xylan increased the least, while xyloglucan

249 cannot be measured, because it directly produced obvious flocculent precipitation

250 with procyanidins. The viscosity and molar mass of hemicellulose were not the main

251 determinants (medium impact) of the strength of the interactions, a result that was

252 consistent with pectins (Liu, Renard, Rolland-Sabaté, & Le Bourvellec, 2021).

253 However, the arabinose sidechain of arabinoxylan did not inhibit the interactions. This

254 observation contrasted with the inhibition of interaction with procyanidins observed

255 for the pectin sidechains. The length of arabinoxylan sidechain composed of only one

256 monosaccharide may be not sufficient to cause spatial site blocking, while it does

257 contribute to decrease rigidity of the backbone.

258 **3.3. Characterization of unbound hemicelluloses and procyanidins**

259 The changes in free hemicelluloses and procyanidins after interaction were

260 explored using supernatants collected after turbidity measurements. After mixing of

261 the two participants (60 mM epicatechin equivalent for procyanidins and 30 mM

262 xylose equivalent for hemicelluloses, a similar concentration for xyloglucan: 7.5 g/L),

263 most of the hemicellulose-procyanidin complexes precipitated, and only a small

264 amount remained in the supernatant. $\overline{M}_w$ values of free hemicelluloses and $\overline{DP_n}$ of

265 free procyanidins exhibited a drastic decrease after interactions (Table 2). This

266 indicated that procyanidin DP9/39 were highly selective for the high molar mass

267 fractions of hemicellulose, especially for xyloglucan. Similarly, hemicelluloses were

268 highly selective for higher $\overline{DP_n}$ of procyanidins, that is, DP39. Moreover,

269 xyloglucan was barely detectable in the supernatant of the DP39-xyloglucan complex

270 solution.

271 Fig. 1 shows the HPSEC-MALLS chromatograms of hemicelluloses that did not

272 form aggregates with procyanidins after interaction. The main peaks of free AXLB

273 and AXMB after interaction with procyanidin DP9 were not significantly different

274 from originals, while after interaction with procyanidin DP39, these main peaks were

275 slightly shifted to higher elution volumes indicating a lower molecular size. The main

276 peaks of free AXLV, AXMV and AXHV similarly shifted to higher elution volumes

277 after interaction with procyanidin DP9 and DP39. Whatever the procyanidins' DP,

278 xyloglucan was barely detectable in the supernatant after interaction, which indicated

279 that procyanidins interacted strongly with it. Finally, xylan lost its first main peak

280 after interaction indicating that procyanidins associated selectively with higher size

281 fraction of xylan (Fig. 1G). Therefore, large-sized hemicelluloses and highly

282 polymerized procyanidins were preferentially aggregated.

283 **Table 2.** Changes in molar mass of hemicelluloses and in the degree of polymerization of procyanidins before and after interactions between xylose-containing
284 hemicelluloses and procyanidins DP9/39.

Sample	Initial hemicelluloses $\bar{M}_w$ * ($\times 10^3$ g/mol)	Unbound hemicelluloses with PCA DP9 $\bar{M}_w$ ($\times 10^3$ g·mol^{-1})	Unbound PCA DP9 with hemicelluloses $\overline{DP_n}$ of free PCA	Unbound hemicelluloses with PCA DP39 $\bar{M}_w$ ($\times 10^3$ g·mol^{-1})	Unbound PCA DP39 with hemicelluloses $\overline{DP_n}$ of free PCA
AXLV	222	130 (-92[a])	8 (-1[b])	125 (-97[a])	25 (-14[b])
AXMV	261	175 (-86)	7 (-2)	162 (-99)	20 (-19)
AXHV	391	244 (-147)	7 (-2)	238 (-159)	18 (-21)
AXMB	257	182 (-75)	6 (-3)	118 (-139)	17 (-22)
AXLB	24	20 (-4)	7 (-2)	16 (-8)	19 (-20)
XYLO	774	NA	6 (-3)	NA	16 (-23)
XYLA	NA	NA	8 (-1)	NA	19 (-20)
Pooled SD	*19.6*	*5.3*	*0.5*	*3.4*	*1.2*

285 *data adapted from Table 1. Average of duplicates for each. $\bar{M}_w$: weight-average molar mass. $\overline{DP_n}$: number-average degree of polymerization. NA: Not applicable. [a] $\Delta \bar{M}_w$:
286 difference of molar mass between hemicellulose unbound to procyanidin solutions after interaction with procyanidins and initial hemicelluloses in buffer. [b] $\Delta \overline{DP_n}$: difference
287 of degree of polymerization between procyanidins unbound to hemicelluloses after interaction with hemicelluloses and initial procyanidins in buffer.
288

3.4. Isothermal Titration Calorimetry (ITC)

ITC provides access to stoichiometric ratios and thermodynamic parameters, e.g., entropy and enthalpy changes, free energy and binding constants during the interactions (Callies & Hernández Daranas, 2016; Liu et al., 2020). This method provides detailed information which complements those derived from turbidity in the detection of interactions. The titration of different hemicelluloses (7.5 and/or 15 mM xylose equivalent, a similar concentration for xyloglucan, ca. 3.75/7.5 g/L) by procyanidin DP9 (30 mM) led to endothermic peaks, but no curve and no titration could be observed (data not shown). Therefore, no interaction could be measured for the procyanidin DP9 using ITC.

Typical thermograms of titration of AXLV, AXMV, AXHV, AXMB, AXLB and xylan (15 mM xylose equivalent, a similar concentration for xyloglucan, ca. 3.75 g/L) titrated by procyanidin DP39 (30 mM (-)-epicatechin equivalent) showed strong exothermic peaks. Blank experiments (procyanidin DP39 injection in buffer) produced only small endothermic peaks, which were subtracted before integration (Supplementary Fig. 1). These ITC titration curves are consistent with previous studies on pectins (Fernandes et al., 2020; Liu, Renard, Rolland-Sabaté, & Le Bourvellec, 2021; Watrelot et al., 2014). However, xyloglucan behaved very differently from arabinoxylan and xylan upon mixing with procyanidin DP39 solution (Fig. 3). The curve was similar to the typical curve of protein-ligand interactions (Poncet-Legrand, Gautier, Cheynier, & Imberty, 2007), with a relatively sharply reduced exothermic peak upon addition of procyanidins. As the concentration of

311   procyanidin increased, the number of available binding sites on xyloglucan decreased

312   until saturation, and the addition of more procyanidin led to a plateau. The mechanism

313   of their interaction may consist of three consecutive stages corresponding to (i) the

314   presence of very few particles, (ii) the formation of xyloglucan-procyanidin

315   aggregates of relatively small size, and (iii) the formation of precipitation upon further

316   addition of procyanidins.
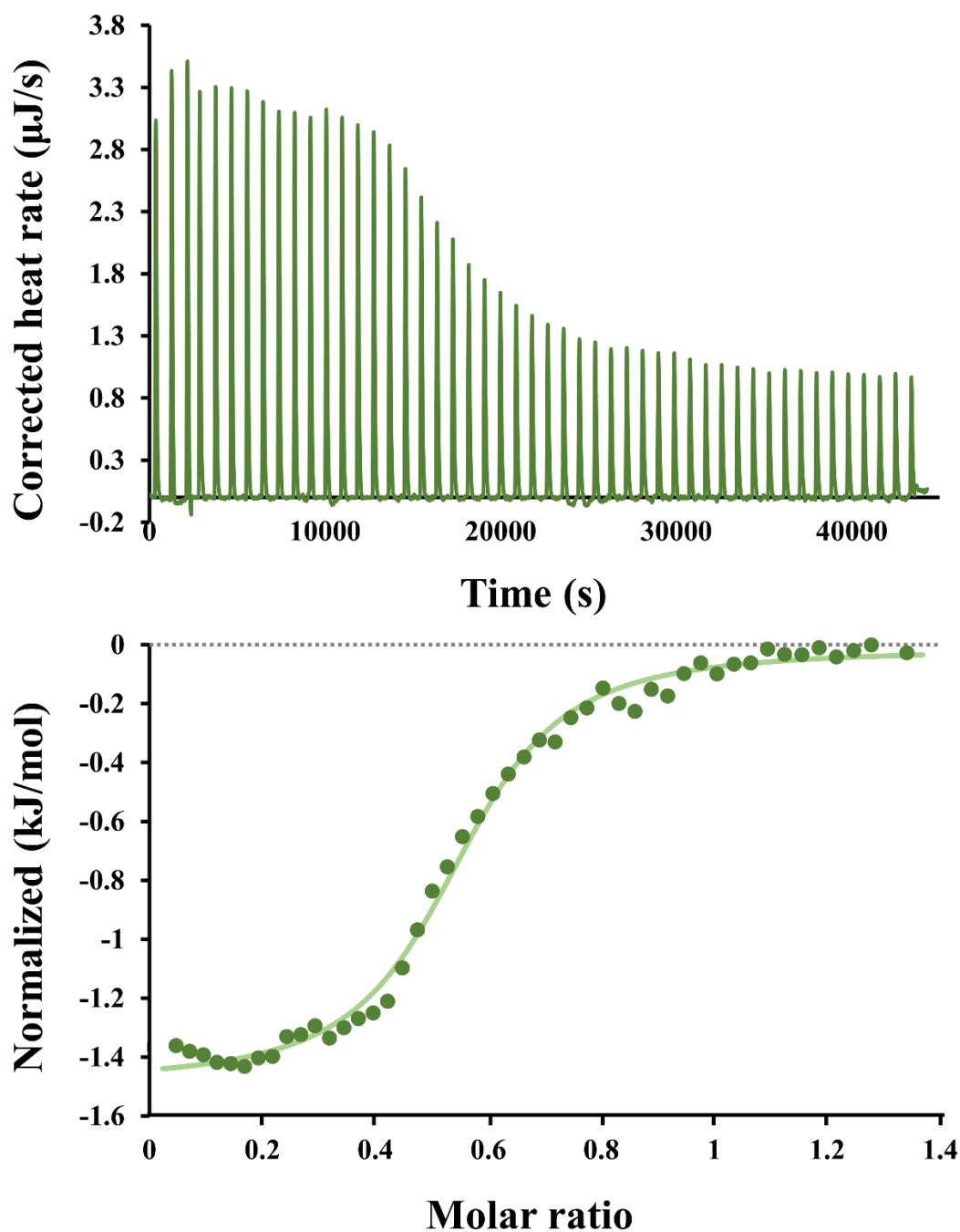
Fig. 3. Thermogram of titration of xyloglucan with procyanidins DP39. The measurement of heat release at the top, while the molar enthalpy changes against (-)-epicatechin/xylose equivalent ratio after peak integration at the bottom.

Table 3. Thermodynamic parameters of interactions measured by ITC: hemicelluloses (15 mM xylose equivalent, 7.5 mM for xyloglucan) and procyanidins DP39 (30 mM (-)-epicatechin equivalent).

DP39	n	K_a (M^{-1})	ΔH (kJ/mol)	ΔS (J/mol/K)	ΔG (kJ/mol)	$-T\Delta S$ (kJ/mol)	Enthalpy (%)	Entropy (%)
AXLV	0.094	5849	-0.31	71.09	-21.50	-21.20	1%	99%

AXMV	0.010	5472	-2.26	63.99	-21.34	-19.08	11%	89%
AXHV	0.089	4509	-0.34	68.81	-20.86	-20.52	2%	98%
AXMB	0.108	4600	-0.22	69.39	-20.90	-20.69	1%	99%
AXLB	0.010	424	-13.65	4.52	-14.99	-1.35	91%	9%
XYLO	0.554	7949	-1.47	69.73	-22.26	-20.79	7%	93%
XYLA	0.107	1452	-0.69	58.19	-18.04	-17.35	4%	96%
Pooled SD	*0.002*	*144*	*0.54*	*0.85*	*0.77*	*0.86*	*-*	*-*

Pooled SD: pooled standard deviation. n: stoichiometry, K_a: affinity level, ΔH, ΔS and ΔG: enthalpy, entropy and free enthalpy, respectively. T: temperature. AXLV: Arabinoxylan (low viscosity); AXMV: Arabinoxylan (medium viscosity); AXHV: Arabinoxylan (high viscosity); AXMB: Arabinoxylan (30% Ara); AXLB: Arabinoxylan (22% Ara); XYLO: Xyloglucan; XYLA: Xylan. Enthalpy (%) = ΔH / (ΔH - TΔS) × 100%; Entropy (%) = - TΔS / (ΔH - TΔS) × 100%. Average of duplicates for each.

Stoichiometry (defined as ratio of (-)-epicatechin/xylose) was c.a. 0.1 for AXLV, AXHV, AXMB and xylan (1 molecule of (-)-epicatechin bound 10 molecules of xylose) and c.a. 0.6 for xyloglucan (1 molecule of (-)-epicatechin bound 2 molecules of xylose) using a one-site model. The association constant ranged between 424 M^{-1} and 7949 M^{-1} and increased in the sequence below: AXLB < Xylan < AXHV ≈ AXMB ≈ AXMV ≈ AXLV < Xyloglucan (Table 3). The affinity range of hemicelluloses binding to procyanidins is between that of whole cell walls ($10^2/10^3$ M^{-1}) and pectins ($10^3/10^4$ M^{-1}) (Brahem, Renard, Bureau, Watrelot, & Le Bourvellec, 2019; Fernandes et al., 2020; Liu et al., 2020; Liu, Renard, Rolland-Sabaté, & Le Bourvellec, 2021). The association constants for strong affinity are generally larger than 10^4 M^{-1} (Turnbull & Daranas, 2003). Xyloglucan with a glucose backbone and xylose side-chains structure, and the highest molar mass, had the highest affinity for procyanidin DP39, indicating that glucose backbone facilitated the interaction with procyanidins. AXLB and xylan with the least arabinose and lower molar mass had lowest affinity for procyanidin DP39. For the other arabinoxylans, although they had

347 different sugar ratios, molar mass and viscosities, their affinities with procyanidins

348 were very close.

349   The strong entropy contribution (-TΔS from -21 to -17 kJ/mol) showed that the

350 interactions between hemicelluloses (except for AXLB) and procyanidins were

351 mostly driven by entropy, i.e., by hydrophobic interactions and the release of water

352 molecules (Liu, Renard, Rolland-Sabaté, & Le Bourvellec, 2021; Poncet-Legrand et

353 al., 2007). The enthalpy contributions were higher for AXLB (ΔH: -14 kJ/mol)

354 indicating that interactions mostly involved hydrogen bonds. The entropy contribution

355 for AXLB was significantly lower than that of other hemicelluloses, which could

356 indicate that the hydrophobic interaction was more significant for their affinity with

357 procyanidins. Generally, pectin has a high affinity for procyanidins, which also due to

358 hydrophobic interaction forces (Liu, Renard, Rolland-Sabaté, & Le Bourvellec, 2021).

359 Therefore, of xylose-containing hemicelluloses, xyloglucan have highest affinity for

360 procyanidins. All other affinities were lower for hemicelluloses with a xylan backbone,

361 especially when the ramification by arabinose was limited. This observation

362 confirmed the results derived from the turbidity experiment. These two methods are

363 complementary, allowing higher sensitivity for detection of the interactions (haze

364 formation) on the one hand and access to stoichiometric ratio and binding enthalpy

365 (ITC) on the other hand. Turbidity measurements provide information on the

366 formation of insoluble complexes, but they can not provide information on the

367 mechanism and binding sites.

368   Furthermore, Phan et al. (2017) found that small polyphenol molecules (e.g.,

catechins and ferulic acid) selectively bind to the relatively hydrophobic and rigid

cellulose, rather than to the more hydrophilic and flexible arabinoxylan or xyloglucan.

This highlighted the role of polyphenol structure, that is, hemicelluloses may

preferentially bind macromolecular procyanidins, because procyanidins can provide

more hydroxyl groups and hydrophobic sites (Liu et al., 2020; Liu, Renard,

Rolland-Sabaté, & Le Bourvellec, 2021).

3.5. Theoretical calculation of the interactions

3.5.1. Reactivity of monosaccharides

Theoretical calculations revealed a mechanism that goes beyond the widely

accepted frontier molecular orbital (FMO) theory, which stated that the frontier

orbitals, that is, the highest occupied molecular orbital (HOMO) and the lowest

unoccupied molecular orbital (LUMO), were mainly responsible for chemical

reactivity (Huang et al., 2020). The smaller HOMO-LUMO gap defined the high

chemical reactivity and polarizability of compounds. Among the different

monosaccharide structural units, glucose and mannose had the relatively lower

HOMO-LUMO gap of 8.10 eV and 8.28 eV, respectively (Supplementary Fig. 2).

Compared with a higher HOMO-LUMO gap of 8.52 eV and 8.53 eV in xylose and

rhamnose, respectively, glucose and mannose units had the higher chemical reactivity

and could more easily interact with other molecules. Xyloglucan contains the highest

proportion of glucose. However, the content of xylose in xylan was the highest, and

the chemical properties of xylose and rhamnose are relatively inactive, making it

difficult for xylan to combine with other molecules to form a complex. For AXLB,

391 AXMB, and AXHB, the structure had a certain regularity: the content of arabinose

392 side-chains gradually increased, while the content of xylose (backbone) gradually

393 decreased. The higher content of xylose, which has less polarizability than the other

394 sugar monomers, explains the lower reactivity of AXLB. However, the reactivity of

395 the atoms on the monosaccharide structure is only one among other factor, and the

396 appropriate relative conformation of hemicelluloses and procyanidins remains the

397 dominant factor that drive the interactions. The backbone of xyloglucan and

398 xylan/arabinoxylan are the glucose and xylose backbone, respectively. In addition,

399 xylans are highly ordered, while arabinoxylans are less ordered and their arabinose

400 substituents influence the degree of rigidity of the structure (Selig, Thygesen, Felby,

401 & Master, 2015; Shrestha et al., 2019).

402 **3.5.2. Structured hemicelluloses**

403 Considering the large number of unit structures and the excessive number of atoms in

404 polymerized procyanidins, it is not possible at current stage for computers to modelize

405 these structures. Therefore, procyanidin B2 was used to model the local interaction

406 between hemicelluloses and procyanidins. The simulation of local interactions is an

407 important guide to subsequent global simulations. The molecular electrostatic

408 potential (ESP) on the molecular van der Waals (vdW) surfaces was calculated and

409 mapped for the five different xylose-containing hemicelluloses and procyanidin B2, in

410 order to gain further understanding of the molecular recognition behavior (Fig. 4).

411 The ESP on the van der Waals surface is appropriate to gather information about the

412 reaction site, molecular property, which is critical for studying and predicting

413 intermolecular interaction (Murray & Politzer, 2011). The pyran ring skeleton (PRS)

414 and CH_2OH group outside the ring presented quite different electrostatic potential

415 characters for different types of hemicellulose. The ESP value over the PRS carbons

416 was moderately negative. As for non-PRS part, that is, CH_2OH group, lone pair of

417 each oxygen atom leads to one or more ESP minima on the vdW surface. Each surface

418 maximum in the non-PRS part corresponds to a hydrogen atom. In addition, the

419 structural optimization of xyloglucan yields the formation of clusters, while

420 hemicelluloses with a xylan backbone still maintain long-chain extension.

421 Lowest-energy conformer after conformation search were kept for further

422 calculations. The optimized binding geometry was meaningful since molecules

423 interact in a complementary manner of the electrostatic potential ESP to form

424 intermolecular interaction. The overall interaction energies in aqueous solution were

425 estimated to be -480, -319, -315, -306 and -246 kJ/mol and -274, -201, -193, -187 and

426 -160 kJ/mol before and after the counterpoise correction, in the cases of procyanidin

427 B2-Xyloglucan, procyanidin B2-AXLB, procyanidin B2-AXMB, procyanidin

428 B2-AXHB and procyanidin B2-Xylan, respectively.

429
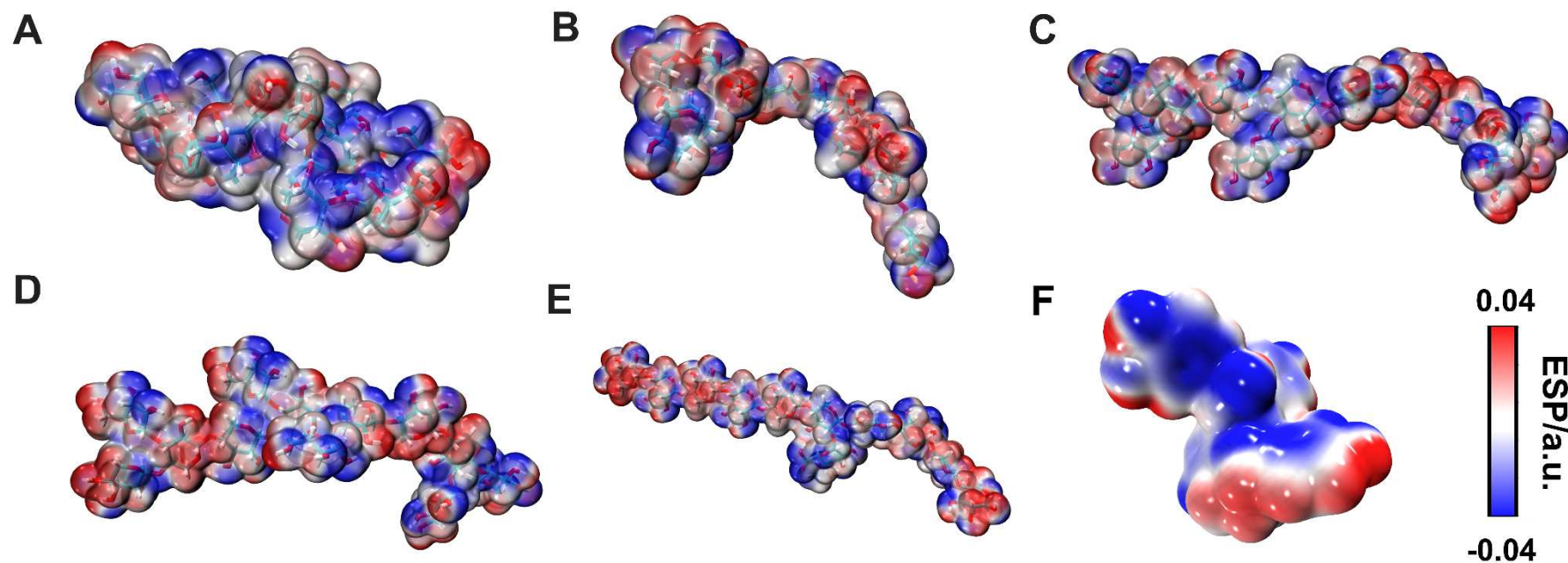
Fig. 4. Molecular electrostatic potential maps. The optimized geometry of the five different hemicellulose compounds at the B3LYP-D3/6-31G(d,p)/SMD (water) level of theory and the molecular electrostatic potential (ESP) analysis results on 0.001 a.u. contours of the electronic density. (A): Xyloglucan, (B): AXLB (22% Ara), (C): AXMB (30% Ara), (D): AXHB (38% Ara), (E): Xylan, (F): Procyanidin B2, respectively. (Blue: negative regions; Red: positive regions). The color scale is also given in a.u.. AXLB: Arabinoxylan (22% Ara); AXMB: Arabinoxylan (30% Ara); AXHB: Arabinoxylan (38% Ara).

434
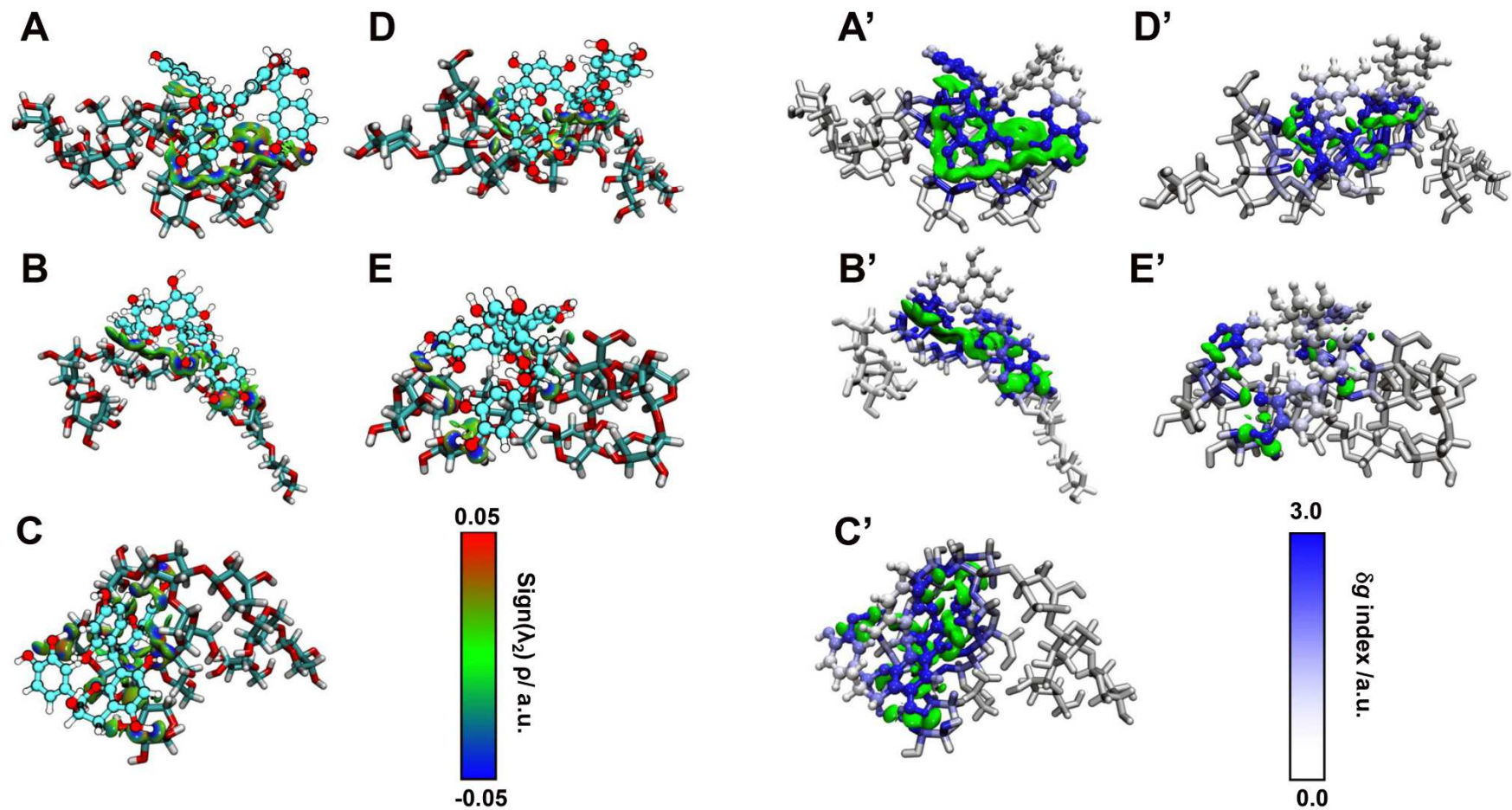
435
Fig. 5. Intermolecular interactions (isosurfaces: 0.05 a.u.) using Independent Gradient Model (IGM) analysis. The non-covalent interaction existed in procyanidin B2
437 and different hemicellulose compounds. Procyanidin B2-Xyloglucan (A), procyanidin B2-AXLB (B), procyanidin B2-AXMB (C), procyanidin B2-AXHB (D) and

438　procyanidin B2-xylan (E). Blue color represented hydrogen bonding interaction, and green represented van der Waals interaction. All isosurfaces are colored

439　according to a BGR (blue-green-red) scheme over the electron density range $-0.05 < \text{sign}(\lambda 2)\, \rho < 0.05$ a.u. Molecular structures were also colored based on atom g

440　indices using IGM analysis for procyanidin B2-Xyloglucan (A'), procyanidin B2-AXLB (B'), procyanidin B2-AXMB (C'), procyanidin B2-AXHB (D') and

441　procyanidin B2-xylan (E') colored according to their contributions to the binding. The relative importance of various atoms in inter-fragment interactions is

442　demonstrated by color intensity. White indicates no contribution to the complexation, and atoms in brighter blue contribute more strongly to the interactions. The

443　green ovals indicate the presence of interactions. AXLB: Arabinoxylan (22% Ara); AXMB: Arabinoxylan (30% Ara); AXHB: Arabinoxylan (38% Ara).

444   Independent gradient model (IGM) analysis revealed the existence of extensive

445   non-covalent interaction occurring between the procyanidin B2 and hemicelluloses.

446   The interactions occur through weak hydrogen bonds (light-blue area in isosurfaces)

447   and van der Waals interactions (green area in isosurfaces). It indicated the vital role of

448   non-covalent contacts facilitating the effective accommodation of target

449   hemicelluloses (Fig. 5). A π-stacking interaction complements the interactions

450   occurring between the aromatic ring of procyanidin B2 and hemicellulose. The main

451   contributions to these complexations occur between procyanidin B2 and

452   hemicelluloses (as schematically enlighten by the colouring of the atoms according to

453   their contribution to the complexation - see Fig. 4). The relative importance of various

454   atoms in inter-fragmentary interaction was demonstrated by using colors, with the

455   atoms in brighter red contributing more strongly to the interactions. In Fig. 4, the

456   volume of the interacting regions could be taken as an indication of the extent of

457   interaction. As a result, procyanidin B2 formed more and less extensive interaction

458   with xyloglucan and xylan residues, respectively, while other hemicelluloses were in

459   the middle. This observation was consistent with the results of the experimental study

460   conducted above. The simulations by Shrestha et al. (2019) showed that the

461   intermolecular interaction with cellulose was not influenced by arabinose side-chain

462   in arabinoxylan.

463   **4. Conclusions**

464   The present study evaluated the nature of the interactions between

465   xylose-containing hemicelluloses, having ether a xylan or a glucan backbone, and

procyanidins by experimental and theoretical methods. Across all methods used, a consistent ranking of the capacity of association with procyanidins emerges as xyloglucan > arabinoxylans > xylan. Hemicelluloses preferentially associate with the high polymerized procyanidin DP39. The various processing-structure-interaction of hemicelluloses and procyanidins could tailor the functional properties of plant-derived products and provide a practical guide to the retention and changes in polyphenols during processing.

Acknowledgements

Conflicts of interest

The authors declare no conflicts of interest.

CRediT authorship contribution statement

Xuwei Liu: Investigation, Software, Formal analysis, Data curation, Writing - original draft. **Jiayi Li**: Software, Formal analysis, Visualization, Writing - review & editing. **Catherine M. G. C. Renard**: Conceptualization, Funding acquisition, Project

487 administration, Validation, Writing - review & editing. **Agnès Rolland-Sabaté**:

488 Supervision, Methods, Software, Formal analysis, Validation, Writing - review &

489 editing. **Serge Perez**: Software, Writing - review & editing. **Carine Le Bourvellec**:

490 Conceptualization, Funding acquisition, Supervision, Validation, Writing - review &

491 editing.

References

492
493 Brahem, M., Renard, C. M. G. C., Bureau, S., Watrelot, A. A., & Le Bourvellec, C.
494   (2019). Pear ripeness and tissue type impact procyanidin-cell wall interactions.
495   *Food Chemistry*, *275*, 754–762. https://doi.org/10.1016/j.foodchem.2018.09.156

496 Callies, O., & Hernández Daranas, A. (2016). Application of isothermal titration
497   calorimetry as a tool to study natural product interactions. *Natural Product*
498   *Reports*, *33*(7), 881–904. https://doi.org/10.1039/c5np00094g

499 Cui, J., Lian, Y., Zhao, C., Du, H., Han, Y., Gao, W., … Zheng, J. (2019). Dietary
500   Fibers from Fruits and Vegetables and Their Health Benefits via Modulation of
501   Gut Microbiota. *Comprehensive Reviews in Food Science and Food Safety*, *18*(5),
502   1514–1532. https://doi.org/10.1111/1541-4337.12489

503 Fernandes, P. A. R., Le Bourvellec, C., Renard, C. M. G. C., Wessel, D. F., Cardoso,
504   S. M., & Coimbra, M. A. (2020). Interactions of arabinan-rich pectic
505   polysaccharides with polyphenols. *Carbohydrate Polymers*, *230*, 115–644.
506   https://doi.org/10.1016/j.carbpol.2019.115644

507 Frisch, M. J., Trucks, G. W., Schlegel, H. B., Scuseria, G. E., Robb, M. A.,
508   Cheeseman, J. R., … others. (2016). Gaussian 16, Revision A. 03, Gaussian, Inc.,
509   Wallingford CT. *City*.

510 Grimme, S., Bannwarth, C., & Shushkov, P. (2017). A Robust and Accurate
511   Tight-Binding Quantum Chemical Method for Structures, Vibrational
512   Frequencies, and Noncovalent Interactions of Large Molecular Systems
513   Parametrized for All spd-Block Elements (Z = 1-86). *Journal of Chemical*
514   *Theory and Computation*, *13*(5), 1989–2009.
515   https://doi.org/10.1021/acs.jctc.7b00118

516 Guyot, S., Marnet, N., Sanoner, P., & Drilleau, J.-F. (2001). Direct thiolysis on crude
517   apple materials for high-performance liquid chromatography characterization
518   and quantification of polyphenols in cider apple tissues and juices. In L. Packer
519   (Ed.), *Methods in Enzymology* (pp. 57–70). Elsevier Inc.
520   https://doi.org/10.1016/S0076-6879(01)35231-X

521   Huang, Q., Li, J., Shi, T., Liang, J., Wang, Z., Bai, L., … Zhao, Y. L. (2020). Defense
522   Mechanism of Phosphorothioated DNA under Peroxynitrite-Mediated Oxidative
523   Stress. *ACS Chemical Biology*, *15*(9), 2558–2567.
524   https://doi.org/10.1021/acschembio.0c00591

525   Jakobek, L., & Matić, P. (2019). Non-covalent dietary fiber - Polyphenol interactions
526   and their influence on polyphenol bioaccessibility. *Trends in Food Science and*
527   *Technology*, *83*, 235–247. https://doi.org/10.1016/j.tifs.2018.11.024

528   Koch, W. (2019). Dietary polyphenols-important non-nutrients in the prevention of
529   chronic noncommunicable diseases. A systematic review. *Nutrients*, *11*(5), 1–35.
530   https://doi.org/10.3390/nu11051039

531   Le Bourvellec, C., Boas, P. B. V., Lepercq, P., Comtet-Marre, S., Auffret, P., Ruiz,
532   P., … Mosoni, P. (2019). Procyanidin—cell wall interactions within apple
533   matrices decrease the metabolization of procyanidins by the human gut
534   microbiota and the anti-inflammatory effect of the resulting microbial
535   metabolome in vitro. *Nutrients*, *11*(3), 664. https://doi.org/10.3390/nu11030664

536   Le Bourvellec, C., Bouchet, B., & Renard, C. M. G. C. (2005). Non-covalent
537   interaction between procyanidins and apple cell wall material. Part III: Study on
538   model polysaccharides. *Biochimica et Biophysica Acta - General Subjects*,
539   *1725*(1), 10–18. https://doi.org/10.1016/j.bbagen.2005.06.004

540   Le Bourvellec, C., Watrelot, A. A., Ginies, C., Imberty, A., & Renard, C. M. G. C.
541   (2012). Impact of processing on the noncovalent interactions between
542   procyanidin and apple cell wall. *Journal of Agricultural and Food Chemistry*,
543   *60*(37), 9484–9494. https://doi.org/10.1021/jf3015975

544   Liu, X., Le Bourvellec, C., Guyot, S., & Renard, C. M. G. C. (2021). Reactivity of
545   flavanols: Their fate in physical food processing and recent advances in their
546   analysis by depolymerization. *Comprehensive Reviews in Food Science and*
547   *Food Safety*, 1–40. https://doi.org/10.1111/1541-4337.12797

548   Liu, X., Le Bourvellec, C., & Renard, C. M. G. C. (2020). Interactions between cell
549   wall polysaccharides and polyphenols: Effect of molecular internal structure.

Comprehensive Reviews in Food Science and Food Safety, *19*(6), 3574–3617. https://doi.org/10.1111/1541-4337.12632

Liu, X., Renard, C. M. G. C., Bureau, S., & Le Bourvellec, C. (2021). Interactions between heterogeneous cell walls and two procyanidins: Insights from the effects of chemical composition and physical structure. *Food Hydrocolloids*, *121*, 107018. https://doi.org/10.1016/j.foodhyd.2021.107018

Liu, X., Renard, C. M. G. C., Rolland-Sabaté, A., Bureau, S., & Le Bourvellec, C. (2021). Modification of apple, beet and kiwifruit cell walls by boiling in acid conditions: Common and specific responses. *Food Hydrocolloids*, *112*, 106266. https://doi.org/10.1016/j.foodhyd.2020.106266

Liu, X., Renard, C. M. G. C., Rolland-Sabaté, A., & Le Bourvellec, C. (2021). Exploring interactions between pectins and procyanidins: Structure-function relationships. *Food Hydrocolloids*, *113*, 106498. https://doi.org/10.1016/j.foodhyd.2020.106498

Lu, T., & Chen, F. (2012). Multiwfn: A multifunctional wavefunction analyzer. *Journal of Computational Chemistry*, *33*(5), 580–592. https://doi.org/10.1002/jcc.22885

Murray, J. S., & Politzer, P. (2011). The electrostatic potential: An overview. *Wiley Interdisciplinary Reviews: Computational Molecular Science*, *1*(2), 153–163. https://doi.org/10.1002/wcms.19

Pérez, S., & Rivet, A. (2021). Polys Glycan Builder: An online application for intuitive construction of 3D structures of complex carbohydrates, in methods in molecular biology. In T. Lutteke (Ed.), *Glycoinformatics: Methods and protocols* (Second Edi).

Pérez, S., Tubiana, T., Imberty, A., & Baaden, M. (2015). Three-dimensional representations of complex carbohydrates and polysaccharides - SweetUnityMol: A video game-based computer graphic software. *Glycobiology*, *25*(5), 483–491. https://doi.org/10.1093/glycob/cwu133

Phan, A. D. T., Flanagan, B. M., D'Arcy, B. R., & Gidley, M. J. (2017). Binding

selectivity of dietary polyphenols to different plant cell wall components: Quantification and mechanism. *Food Chemistry*, *233*, 216–227. https://doi.org/10.1016/j.foodchem.2017.04.115

Poncet-Legrand, C., Gautier, C., Cheynier, V., & Imberty, A. (2007). Interactions between flavan-3-ols and poly(L-proline) studied by isothermal titration calorimetry: Effect of the tannin structure. *Journal of Agricultural and Food Chemistry*, *55*(22), 9235–9240. https://doi.org/10.1021/jf071297o

Pracht, P., Bohle, F., & Grimme, S. (2020). Automated exploration of the low-energy chemical space with fast quantum chemical methods. *Physical Chemistry Chemical Physics*, *22*(14), 7169–7192. https://doi.org/10.1039/c9cp06869d

Renard, C. M. G. C., Watrelot, A. A., & Le Bourvellec, C. (2017). Interactions between polyphenols and polysaccharides: Mechanisms and consequences in food processing and digestion. *Trends in Food Science and Technology*, *60*, 43–51. https://doi.org/10.1016/j.tifs.2016.10.022

Rolland-Sabaté, A., Colonna, P., Potocki-Véronèse, G., Monsan, P., & Planchot, V. (2004). Elongation and insolubilisation of α-glucans by the action of Neisseria polysaccharea amylosucrase. *Journal of Cereal Science*, *40*(1), 17–30. https://doi.org/10.1016/j.jcs.2004.04.001

Ruiz-Garcia, Y., Smith, P. A., & Bindon, K. A. (2014). Selective extraction of polysaccharide affects the adsorption of proanthocyanidin by grape cell walls. *Carbohydrate Polymers*, *114*, 102–114. https://doi.org/10.1016/j.carbpol.2014.07.024

Saura-Calixto, F., & Pérez-Jiménez, J. (2018). *Non-extractable Polyphenols and Carotenoids*. (F. Saura-Calixto & J. Pérez-Jiménez, Eds.) (Vol. 5). Royal Society of Chemistry. https://doi.org/doi.org/10.1039/9781788013208

Seal, C. J., Courtin, C. M., Venema, K., & de Vries, J. (2021). Health benefits of whole grain: effects on dietary carbohydrate quality, the gut microbiome, and consequences of processing. *Comprehensive Reviews in Food Science and Food Safety*. https://doi.org/10.1111/1541-4337.12728

608 Selig, M. J., Thygesen, L. G., Felby, C., & Master, E. R. (2015). Debranching of
609   soluble wheat arabinoxylan dramatically enhances recalcitrant binding to
610   cellulose.   *Biotechnology   Letters*,   *37*(3),   633–641.
611   https://doi.org/10.1007/s10529-014-1705-0

612 Shrestha, U. R., Smith, S., Pingali, S. V., Yang, H., Zahran, M., Breunig, L., …
613   Petridis, L. (2019). Arabinose substitution effect on xylan rigidity and
614   self-aggregation.   *Cellulose*,   *26*(4),   2267–2278.
615   https://doi.org/10.1007/s10570-018-2202-8

616 Turnbull, W. B., & Daranas, A. H. (2003). On the value of c: Can low affinity
617   systems be studied by isothermal titration calorimetry? *Journal of the American
618   Chemical Society*, *125*(48), 14859–14866. https://doi.org/10.1021/ja036166s

619 Waskom, M. (2014). Seaborn: Statistical Data Visualization. Retrieved from
620   http://stanford.edu/~mwaskom/software/seaborn/

621 Watrelot, A. A., Le Bourvellec, C., Imberty, A., & Renard, C. M. G. C. (2013).
622   Interactions between pectic compounds and procyanidins are influenced by
623   methylation degree and chain length. *Biomacromolecules*, *14*(3), 709–718.
624   https://doi.org/10.1021/bm301796y

625 Watrelot, A. A., Le Bourvellec, C., Imberty, A., & Renard, C. M. G. C. (2014).
626   Neutral sugar side chains of pectins limit interactions with procyanidins.
627   *Carbohydrate   Polymers*,   *99*,   527–536.
628   https://doi.org/10.1016/j.carbpol.2013.08.094

629
630
631